AIAA 81-1266R

Viscous-Inviscid Interaction for Transonic Wing-Body Configurations Including Wake Effects

Craig L. Streett*
NASA Langley Research Center, Hampton, Va.

An existing three-dimensional compressible integral boundary-layer method was modified to account for mean dilatation effects, to model transition properly, and to provide better numerical stability near computational boundaries. Results of this method were compared against those from a three-dimensional finite-difference boundary-layer method on a difficult test case. An interaction procedure was developed to couple this integral method with a number of wing-alone and wing-body transonic potential codes to account for viscous effects. A strip wake model, including thickness and curvature effects, was developed and incorporated into this interaction procedure. Results from this procedure were compared against experimental data and results from previous procedures, on test cases where viscous effects were large.

Nomenclature

a_e = speed of sound at edge of boundary layer
a_0 = stagnation speed of sound
c = local chord length
C_ℓ = local section lift coefficient
G = reduced potential used in inviscid codes
H = streamwise shape factor, $\equiv \delta_1^*/\theta_1$
M = Mach number
R = normalized lift reduction due to viscous effects
Re = Reynolds number/unit length
S_w = arc length along wake
u = local boundary-layer velocity in the external streamwise direction
U = external velocity magnitude
v = local boundary-layer velocity normal to the external streamwise direction
x = chordwise coordinate
y = spanwise coordinate
z = physical normal coordinate
Z = transformed normal coordinate
α = angle of attack
β = angle between external streamline and wall shear direction
Γ_w = wake vorticity/potential jump
Δ = transformed boundary-layer thickness
δ^* = total boundary-layer displacement thickness
δ_1^* = streamwise displacement thickness,

$$\equiv \int_0^\infty \left(1-\frac{\rho}{\rho_e}\frac{u}{U}\right)dz$$

δ_2^* = cross flow displacement thickness, $\equiv \int_0^\infty \frac{\rho}{\rho_e}\frac{v}{U}dz$

δ_w^* = wake displacement thickness,

$$\equiv \int_{-\infty}^\infty \left(1-\frac{\rho}{\rho_e}\frac{u}{U}\right)dz$$

η = normalized spanwise coordinate, $\equiv y/c$
ϵ = local flow angle in a constant-span plane
κ_w = wake curvature
ρ = local density
ρ_e = density at edge of boundary-layer wake
ρ_0 = stagnation density
θ_1 = streamwise momentum thickness,

$$\equiv \int_0^\infty \frac{\rho}{\rho_e}\frac{u}{U}\left(1-\frac{u}{U}\right)dz$$

θ_w = wake momentum thickness,

$$\equiv \int_{-\infty}^\infty \frac{\rho}{\rho_e}\frac{u}{U}\left(1-\frac{u}{U}\right)dz$$

Presented as Paper 81-1266 at the AIAA 14th Fluid and Plasma Dynamics Conference, Palo Alto, Calif., June 23-25, 1981; submitted July 14, 1981. This paper is declared a work of U. S. Government and therefore is in the public domain.

*Aero-Space Technologist, Theoretical Aerodynamics Branch, Transonic Aerodynamics Division. Member AIAA.

Introduction

IT generally is recognized now that any analysis procedure for computing transonic flow over wing and wing-body configurations must include some form of viscous correction on the wing to give reasonable agreement with experiment. In the past, a number of researchers have shown good agreement without viscous correction through the use of lift matching; however, such techniques require a priori knowledge of the overall lift, rather than resulting naturally from the computation. Ideally, one would like to compute flows using only known geometric quantities and flow conditions. Some form of viscous correction thus appears to be required.

Techniques of solving the Navier-Stokes equations, either in full form or in some reduced form (parabolized, velocity split, etc.), are still in their infancy. In addition, Navier-Stokes computations for a transonic wing at Reynolds numbers of interest as yet are beyond the capability of present computers. Alternatively, potential flow and boundary-layer computational techniques are mature, and the viscous/inviscid interaction philosophy of computing flowfields with viscous effects has been applied successfully to problems of interest in the past.

Viscous/inviscid interaction is defined herein as the iterative solving of the boundary-layer and potential (or other inviscid) equations, coupled through the concept of boundary-layer displacement thickness. If the Navier-Stokes equations are written in terms of matched asymptotic expansions near and far from a wall, it can be shown that to $0(Re^{-1/2})$ the pressure on the wall is determined from the solution of the outer (inviscid) equations, with the flow tangency boundary condition displaced from the wall by a distance determined from the inner (boundary-layer) equations. The viscous-inviscid interaction technique produces a uniformly valid solution, with the exception of strong interaction regions; e.g., near the trailing edge, a normal shock, or the wing tip.

Melnik[1] has shown in two dimensions that this interaction of the first-order equations involves a singularity in the pressure gradient and streamline curvature at the trailing edge

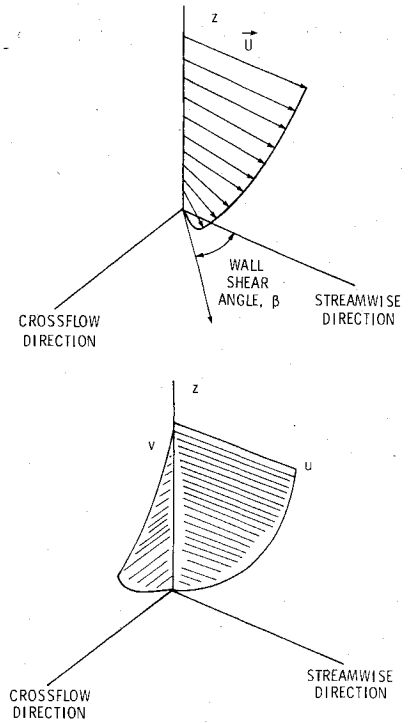

Fig. 1 Breakdown of three-dimensional boundary layer into components.

of an airfoil. It has been demonstrated computationally, however, that iterating the boundary layer and potential equations until convergence produces a solution in which this singularity does not appear. Although this self-consistent solution is not singular, it is inconsistent with the normal momentum equation in a small region near the trailing edge. Correction to the inviscid boundary conditions near the trailing edge in two dimensions was developed in Ref. 1 to account for this singularity; a similar development for three-dimensional wings with spanwise flow at the trailing edge is not available. Although self-consistent interaction solutions are not rigorously accurate to first order near the trailing edge, such solutions do show good agreement with experiment. Such a self-consistent development is described in this paper. It will be shown in this paper that, by including the effects of wing surface boundary layer and wake displacement and curvature, wing lift distribution and shock position are predicted well. However, since the strong viscous-inviscid interaction of the trailing-edge region is not modeled properly, trailing-edge pressures are generally predicted too high. The drag predicted by this method, which accounts only for weak interaction, thus is in error. It is shown in Ref. 1 for two-dimensional airfoil flow that the trailing-edge strong interaction region must be accounted for to obtain accurate drag prediction.

Boundary-Layer Method and Verification

Boundary-Layer Analysis

The boundary-layer method used in this study was obtained from Dornier GmbH; it is based on the laminar scheme developed in Ref. 2 and the turbulent method described in Ref. 3, with a number of modifications. Details of the development of these schemes will not be given here; rather, a general description and discussion of assumptions and their effects follow.

For purposes of analysis, the boundary layer is decomposed into components parallel and perpendicular to the external streamline. A basic schematic of this decomposition of the boundary layer is shown in Fig. 1. The situation shown is that most commonly encountered, in which the cross flow velocity does not change sign across the boundary layer.

The laminar analysis used in this study basically is unchanged from that developed in Ref. 2. The streamwise velocity profile is assumed to be of the Faulkner-Skan family of similarity profiles. The cross flow profile is generated from a linear combination of these similarity profiles; this combination is capable of generating profiles with cross flow velocity crossover. These profiles are defined for incompressible flow; the Stewartson transformation is used to scale the normal coordinate

$$dZ = (\rho a_e/\rho_0 a_0)\,dz$$

By this transformation, the compressible velocity profile may be represented by the incompressible form, as a function of the transformed variable Z.

These profile assumptions are substituted into the two boundary-layer momentum equations and their corresponding moment of momentum relations. The moment relations are often used in integral boundary-layer methods[4]; they are independent relations formed by multiplying the momentum equations by the corresponding velocity component. These four equations are then integrated from the wall to the boundary-layer edge. The resultant equations form a system of four coupled partial-differential equations in two dimensions on the surface of the wing for four unknowns; the four unknowns are parameters related to the streamwise momentum thickness, the wall shear, the cross flow displacement thickness, and the boundary-layer thickness. The streamwise momentum thickness is defined as

$$\theta_1 = \int_0^\infty \frac{\rho}{\rho_e}\frac{u}{U}\left(1-\frac{u}{U}\right)dz$$

and the cross flow displacement thickness as

$$\delta_2^* = \int_0^\infty \frac{\rho}{\rho_e}\frac{v}{U}\,dz$$

In the turbulent case, a simple power-law profile is assumed for the streamwise direction, in the form

$$\frac{u}{U} = \left(\frac{Z}{\Delta}\right)^{n(\bar{H})}$$

where Z is again the transformed normal coordinate, and the exponent n is a function of the streamwise shape factor $\bar{H}$. The cross flow profile used was suggested by Mager[5]

$$\frac{v}{U} = \frac{u}{U}\left(1-\frac{Z}{\Delta}\right)^2\tan\beta$$

where β is the angle between the external streamline and the wall shear direction. Note that this relation cannot predict a cross flow profile with velocity crossover.

These profiles are substituted into the boundary-layer momentum equations and integrated, as before; a modified Ludwieg-Tillmann relation is used to evaluate the wall shear.[6] To close the system of equations, an integral continuity equation is formed, in which the change in mass flow in the boundary layer is identified explicitly. This change in mass flow, the so-called entrainment coefficient, is related to the other integral quantities through the lag-entrainment concept of Green et al.[7] Thus, in the turbulent case, a set of three coupled first-order partial-differential equations is generated for the streamwise momentum thickness, the shape factor, and the wall shear angle. The use of the lag-entrainment

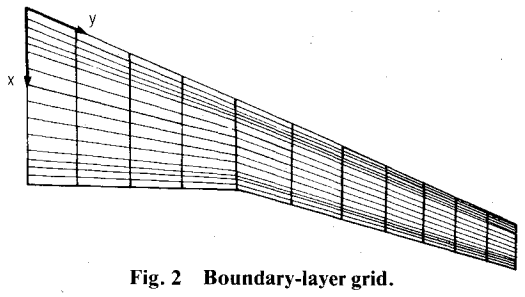

Fig. 2 Boundary-layer grid.

relations, rather than a local entrainment equation is the difference between the method used in this study and that described in Ref. 3.

For a three-dimensional boundary layer, the displacement thickness must be computed as a solution to a partial-differential equation on the surface, rather than being computed from a local integral as in the two-dimensional case. In both the laminar and turbulent methods, therefore, an a posteriori solution of the integrated continuity equation yields the displacement thickness.

Rather than using a streamline coordinate system, as is usually done in three-dimensional boundary-layer calculations, a simple constant-chord fraction, constant span line coordinate system is used. A schematic representation of the coordinate system used is given in Fig. 2. Although nonorthogonal, this system alleviates the difficulty of having to generate a complex new coordinate system for each viscous-inviscid iteration. The additional terms from the nonorthogonal transformation are not time-consuming computationally, since the systems of equations are first order, so this coordinate system is considered more efficient than streamline coordinates for the integral methods.

The three-dimensional boundary-layer equations display hyperbolic properties in the planform plane; that is, at any point on the plane, the equations have a domain of dependence which must be honored in any numerical solution scheme. The integral equations have the same property. It is shown in Ref. 8 that the characteristics of the turbulent integral equations always lie between the external streamline and the wall shear line, giving a convenient, conservative approximation to the exact domain of dependence.

An explicit finite-difference scheme is used to march the solution of the coupled system of equations in the chordwise direction. Differencing of quantities in the y (spanwise) direction must be upwind to account for the domain of dependence properly. That is, if both the external streamline and the wall shear line extend to the same side of the chord line from a computational point, the spanwise difference must be taken as one sided from the opposite side. If the external streamline and wall shear line lie on opposite sides of the chord line, a central difference is used for the spanwise derivative. In addition, the step size in the x (chordwise) direction is limited by the Courant-Friedricks-Lewy (CFL) condition, a necessary condition for the stability of an approximate solution scheme for a hyperbolic equation.[9]

The spanwise differencing scheme of Ref. 8 must be modified at the wing root and tip, where flow into the computational region occurs at these boundaries, in order to make the procedure more reliable. Strictly, initial conditions must be provided at these locations. None being available, conditions along the boundaries must be assumed in these cases, if the numerical scheme is to be stable. At the wing root, a plane of symmetry is assumed. Thus, on the chord line the cross flow velocity is set to zero, as are all spanwise derivatives. Such an assumption is at least a reasonable model of the physical situation. The wing-tip boundary is considerably more difficult. For this study, the assumption of zero spanwise derivatives on the tip chord line is used when flow into the region along this boundary is signaled. This is equivalent to assuming locally that the tip is part of an infinite swept wing. This assumption was found to be the weakest condition of those examined that was always stable and gave the least disturbance across the span.

The initial condition along the leading edge is provided by an approximate attachment line analysis, such as contained in Ref. 10. The attachment line is assumed to be along the wing leading edge. Transition location is input, fixed along a span line at that fraction chord distance. The transition model was modified from the original boundary-layer code obtained from Dornier to enforce continuity of the displacement thickness at transition. There is no inconsistency in this assumption as there would be in many two-dimensional integral methods, as δ^* is not an integral parameter of either the laminar or the turbulent method, but is developed from a separate integration of the continuity equation.

Separation is signaled in the streamwise direction when integral parameters reach critical values; in the laminar case, when the transformed wall shear reaches zero; and, in the turbulent case, when the streamwise shape factor reaches 2.4. No cross flow separation model is used. When laminar separation is detected along a chord line, transition is assumed over the entire span. If separation is signaled at a point in a turbulent region, the streamwise shape factor, skin friction, and wall shear angle are frozen thereafter along that chord line, and spanwise derivatives are set to zero. A one-dimensional integration of the integral equations is thereafter performed on this chord line. This is considered an extrapolation technique; it should be understood that the integral equations with the given profile assumptions are invalid in large regions of separation. However, this method is assumed to give at least a reasonable solution in this situation and is required since such separated regions often appear during the early iterations of the viscous-inviscid interaction. Were the boundary-layer method to stop at separation, the iteration procedure could not continue. If the interaction scheme converges to a solution with large separation regions remaining, the underlying assumption of the existence of a thin viscous region is invalid.

Modifications were also made to the lag-entrainment calculations, in order to improve the δ^* predictions. First, the streamwise pressure gradient was incorporated correctly into the equations that originally were developed for the two-dimensional case. Second, a modification to the dissipation length scale, due to dilatation of the compressible flow, was applied.[7] The effects of these modifications are only seen in regions of severe pressure gradient or large cross flow.

Verification of Boundary-Layer Method

In order to gain confidence in the integral boundary-layer method, a rather severe test case was run for comparison with results from the three-dimensional finite-difference boundary-layer method described in Ref. 11. The velocity data input of both boundary-layer codes was a final converged interacted solution for the flow about a swept, tapered transport wing with significant aft camber. The interaction procedure used to produce this solution is the topic of later sections of this paper; details of this procedure are not important here. A converged solution was used as input since the finite-difference code of Ref. 11 was unable to produce a boundary-layer solution over so much of the wing surface that comparisons were meaningless when the inviscid, uninteracted velocity distribution was input.

Figure 3 shows the difference in the displacement thickness predictions of the original Dornier three-dimensional integral boundary-layer code and the code modified for use in this study. Differences are seen near transition (which for this case occurred at $0.17c$), after the shock near midchord on the upper surface, at the upper surface trailing edge, and in the cove region on the lower surface.

A comparison of the displacement thickness predictions of the modified integral method and of the finite-difference

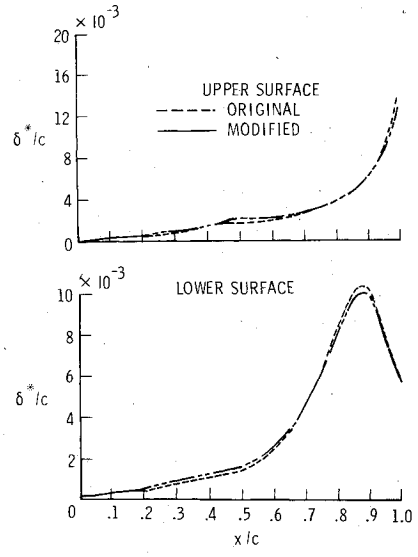

Fig. 3 Comparison of displacement thickness predictions, original and modified integral methods, $\eta = 0.6$.

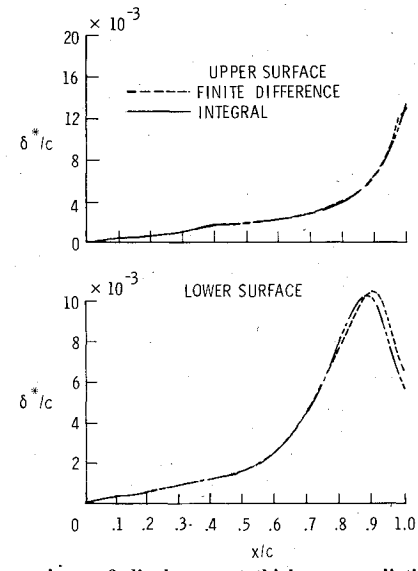

Fig. 4 Comparison of displacement thickness predictions, present integral and finite difference methods, $\eta = 0.7$.

scheme of Ref. 11 is given in Fig. 4. The span station at which this comparison is made is near midspan, since assumptions made at the wing root and tip are different for the two methods. The agreement shown at this midspan station is typical for most of the wing. The largest percent difference is just aft of the midchord shock. The two methods also agree well on the location of the small upper surface trailing-edge separation region and on the wall shear angle in the lower surface cove region. Even the skin-friction coefficient predicted by the integral method is within 10% of that predicted by the finite-difference code, despite the very crude skin-friction model used in the integral method. The finite-difference code required almost 3200 CP seconds on the CDC CYBER 173 to produce a boundary-layer solution for this test case, whereas the integral code required less than 1/30 of this time and used about half the core storage.

Results of the three-dimensional integral boundary-layer method were also compared against experimental data. Although three-dimensional test cases were desired, cases with adequate coverage of velocity data could not be found. In principle, the two momentum equations and the continuity equation could be solved in the planform plane at the edge of

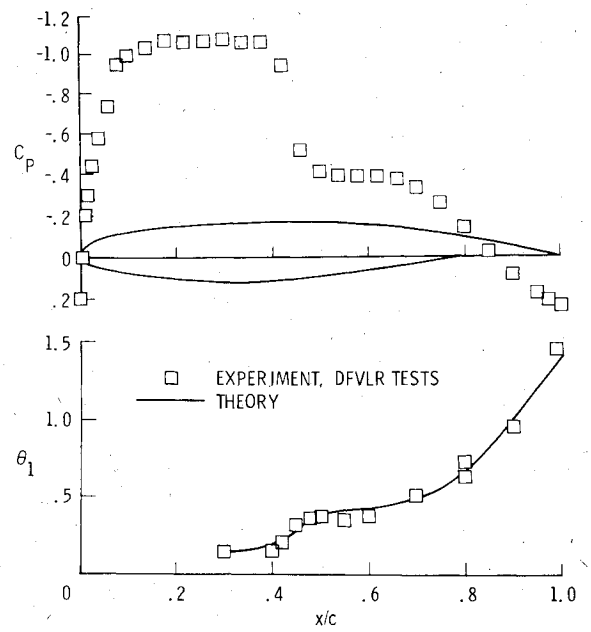

Fig. 5 Two-dimensional boundary layer only, comparison with experiment, $M = 0.76$, Reynolds number based on chord $= 2.4 \times 10^6$.

the boundary layer to derive the external velocity distribution given the surface pressure. However, such a scheme requires fixing a set of rather arbitrary boundary conditions, especially at the critical tip region which can be an inflow boundary for the upper surface. In addition, the equations are first order and were found to be quite sensitive to the applied boundary conditions; this scheme was thus dropped after some effort, and some two-dimensional test cases were run.

Perhaps the most representative and difficult two-dimensional test case was that of the upper surface boundary layer on the CAST 7 airfoil as tested in the DFVLR 1×1-m tunnel.[12] The case included a moderately strong shock and some separation at the trailing edge. The test and calculation were run at a Mach number of 0.76 and a Reynolds number of 2.4×10^6. Calculation was begun from measured momentum thickness and shape factor at 30% chord. Figure 5 shows the measured pressure distribution and the measured and computed momentum thickness distributions. The rapid thickening of the boundary layer in the high adverse pressure gradient region of the shock is predicted well, as is the thickness at the trailing edge. Proper prediction at the trailing edge is quite important, as lift is greatly influenced by the trailing-edge angle of the displacement body. Note the slight post-shock disagreement, perhaps due to the lack of a proper shock-boundary-layer interaction model. However, since the experiment shows the thickness reducing in a region of zero pressure gradient, one must also suspect some three-dimensional relief in the experiment, perhaps the shock curving back near the sidewalls.

Although the physical modeling of the boundary-layer flow is far more accurate in finite-difference methods, it is felt that this integral method, capable of producing solutions in reasonable agreement with a good finite-difference code in far less computer time, is a powerful tool for engineering calculations. Predictions of the integral method also agree well with experiment. The advantage of greatly reduced computation time, along with considerable robustness, makes the integral boundary-layer method well suited for use in interaction schemes.

Inviscid Analyses

During the course of this study, the boundary-layer method described in the previous section was interacted with a number of inviscid analysis codes. The three codes primarily used were

of the FLO series, authored mainly by Jameson and Caughey.[13-16] All three solve the full-potential equation, but in different forms or in different coordinate systems. This study was initiated using FLO-22, written for "wing only" configurations; no results for interactions using FLO-22 are presented in this paper. FLO-27, a wing-cylinder code, and FLO-30, a more general wing-body analysis code were also used. Most of the interacted results presented here will be using FLO-30.

FLO-22 is the oldest code, and thus is somewhat more well-tried than the others. The boundary-conforming grid used in FLO-22 is produced by shearing out the wing sweep and thickness and then applying a parabolic mapping. A planar vortex sheet is assumed. The full-potential equation is written in a nonconservative finite-difference form, using Jameson's "locally-rotated"[16] operators. Solution is by line successive over-relaxation (LSOR) with user-preset grid halving. As with all potential equation methods, good approximation is expected only in flows with weak shocks. Also, the nonconservative formulation produces solutions which do not maintain mass conservation through a shock. The effect of nonconservative form is usually seen in incorrectly predicted shock position.

FLO-27 uses a finite-volume scheme to produce conservative differencing of the full-potential equation. The grid is generated in a manner similar to that in FLO-22, although another shearing transformation is applied to remove wing taper to maintain a constant number of grid points at each span station. Solution is again by LSOR, with additional iterative damping in the form of the mixed space-time derivative added to stabilize the scheme. Although the difference form used in FLO-27 is a better approximation than that in FLO-22, convergence is somewhat slower. Also, the finest grid used in FLO-27 is coarser than that in FLO-22 although FLO-27 requires more core storage. In all, FLO-27 was found to be about 10% more expensive to run than FLO-22 in these interaction studies.

Most of the interaction logic was developed and initial operating experience was gained using FLO-27 for inviscid analysis. As will be shown later, however, the effect of the body on the inviscid flow is large for practical configurations. This necessitated the application of the developed interaction logic to a wing-body analysis code; FLO-30 was obtained for this purpose. The differencing and solution of the full-potential equation as used in FLO-30 is quite similar to that in FLO-27, in which a finite-volume scheme in conservative form is used. The coordinate system used, described in Ref. 15, is termed the "wind-tunnel" grid. Coordinates in the cross flow plane are cylindrical, normalized with the fuselage section variation sheared out. A conformal mapping is used to "unwrap" constant radius surfaces about the wing/wake surface similar to parabolic coordinates. As a last step in the grid-generation procedure, the wing thickness is sheared out. As with all finite-volume coordinate systems, grid extent is finite.

The potential codes described require very large amounts of computer storage. The finest grids used in FLO-22, -27, and -30 were $(192\times24\times32)$, $(161\times18\times35)$, and $(161\times24\times32)$, respectively. Because of this, the integral boundary-layer code and interpolating codes required to process velocity and displacement thickness data were kept as separate routines. The interaction iteration and flow of information between these programs were controlled by a job stream using the CDC CYBER Control Language (CCL).

In order to model the effect of the boundary layer on the outer inviscid flow, the displacement thickness computed by the boundary-layer method was added to the basic wing shape in the surface normal direction. This technique was used, as opposed to using surface transpiration boundary conditions, for simplicity of incorporation into the FLO codes. The techniques are mathematically equivalent to $0(Re^{-1/2})$,[17,18] although some researchers have reported differences in results in practice.[19] The displacement thickness distribution is under-relaxed between iterations to prevent oscillations in total lift and lift distribution in the inviscid calculations. In addition, chordwise constant-value extrapolation is sometimes used on the first iteration when separation is predicted in the cove region of the lower surface; this was found to speed convergence greatly in difficult cases.

The wake in the FLO codes is modeled as a contact discontinuity, across which the pressure is continuous but tangential velocity discontinuous. The small-disturbance form of this condition leads to a constant potential jump being carried downstream from the trailing edge on constant-span lines, with the value of the potential jump determined using potential values at the trailing edge. An approximate wake centerline shape is used, dependent on the wing trailing-edge angle, and is sheared out along with the wing surface shape during the coordinate generation process. This fixes the wake along a coordinate surface, simplifying the application of the wake boundary conditions.

Wake Treatment

One major purpose of this work was to study the effect of the wake approximation used. A full, asymptotically correct wake treatment for three-dimensional wing configurations, of the kind described in Ref. 1 for two dimensions, is at the present time lacking. However, displacement and curvature were the first wake effects accounted for in the two-dimensional studies[17] so a similar treatment is given here.

For this study, the wake model used in the original FLO-30 code was replaced with one satisfying flow tangency on the wake displacement body and the pressure jump condition from wake curvature. As on the wing surface, the solid displacement surface model was used for the wake, constructed in two-dimensional strips. The pressure jump across the wake displacement body, related to the streamline curvature and momentum thickness of the wake, was reformed into a condition on the change in potential jump along the wake, as in Ref. 1.

A fixed approximation to the wake centerline location was used for simplicity. This surface leaves the trailing edge smoothly at the average local trailing-edge angle, and the angle between the wake centerline surface and freestream decays logarithmically, as the general streamline shape of a point vortex in uniform flow. Wake displacement thickness was then applied along this surface.

The flow curvature at the actual wake was computed from the rate of change of the flow angle along the fixed wake; i.e.,

$$\kappa_w = \frac{\mathrm{d}\epsilon}{\mathrm{d}S_w}$$

Here, as in Ref. 1, the approximation is made that the actual wake lies close to the preset inviscid wake near the trailing edge, where the curvature effect is significant. An alternate approximation from inviscid theory was tried

$$\kappa_w = -\left(\frac{1}{u}\frac{\mathrm{d}u}{\mathrm{d}Z}\right)_w$$

where Z is the direction normal to the wake. It was found, however, that the cell spacing in the normal direction was too large, and the curvature computed from the expression was too low near the trailing edge. Since the wake curvature effects are largest in this region, the normal derivative expression for the curvature was dropped. Following Ref. 1, the wake potential jump condition is

$$\frac{\mathrm{d}\Gamma_w}{\mathrm{d}S_w} = -\theta_w\kappa_w$$

with $\Gamma_w = [\,|\,G\,|\,]_w \equiv G_u - G_\ell$ at the wake where the subscripts u and ℓ indicate the upper and lower, respectively.

The integral properties of the wake were computed during the same stage of the interaction iterations as the boundary-layer calculations. A compressible lag-entrainment method, outlined in Ref. 7, was used to compute δ_w^* and θ_w on streamwise strips, using boundary-layer conditions along the trailing edge as initial conditions. Two separate wake computations were made at each span station, for either side of the wake centerline; the total integral properties of the wake are then the sum of the corresponding properties from both sides.

Interaction Procedure

Viscous-inviscid interacted results were produced in this study by iterating potential, boundary-layer, and wake solutions until overall convergence is obtained. A cycle, or "global iteration" of this process, consists of computing the external inviscid flow over the displacement surface of the wing and wake, with the inviscid wake potential jump condition modified by the curvature condition described earlier, and subsequently updating the viscous parameters by boundary layer and wake calculations, using the external velocity distributions previously computed. The updated viscous parameters then provide a new displacement surface for the inviscid calculation of the next global iteration. In practice, the displacement surface updates must be underrelaxed with the viscous parameters of prior cycles to minimize oscillations. The computed displacement thickness on the wing is smoothed to give the displacement surface continuous curvature. Also, the inviscid calculations within each global iteration are stopped short of convergence within the potential equation iterative solution scheme. This was found to reduce the overall work involved in achieving global convergence.

Results

Experimental Configuration

In order to show the advantages of the present more complete wake treatment, as opposed to the treatments previously used for three-dimensional wing calculations, configurations for which viscous effects are large must be used. The first test case chosen was selected from a family of supercritical wings for advanced transport configurations tested in the NASA Langley 8-ft transonic pressure tunnel.[20] The specific wing-body configuration used here is also one of the cases given in Ref. 21; the data for this case are for early domestic dissemination (FEDD) restricted, so results will be presented here without scales. A line drawing of the configuration is given in Fig. 6. The wing is of relatively high-aspect ratio and is swept and tapered. Supercritical sections with large aft camber are used over the span; a small amount of twist is employed, and the thickness ratio varies from 0.144 at the root to 0.106 at the tip. The wing is mounted in a low position on a relatively wide body.

In the second test case presented, a somewhat lower-aspect-ratio wing is midmounted on a cylindrical fuselage. A schematic of this configuration is shown in Fig. 7. Viscous effects for this case are less than on the first test case configuration, but a shock of greater strength appears on the upper surface for similar freestream Mach number and overall lift level. The same airfoil section is used throughout the span, and the wing is slightly twisted. Data for this case were presented in Ref. 22; this configuration is denoted wing "A" midmounted, in that reference.

Basic Computational Results

The flow about the first configuration was computed using FLO-30 alone (i.e., inviscid calculation) and using FLO-30 interacted with the integral boundary-layer scheme, with and without the viscous wake model. The cases were run at the

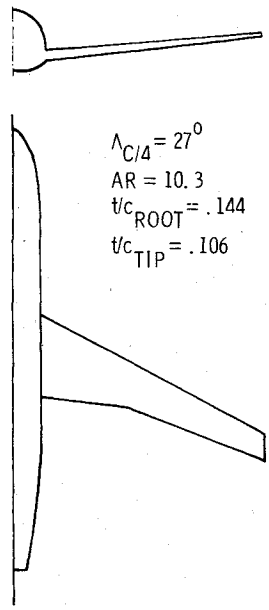

Fig. 6 Advanced transport test case configuration.

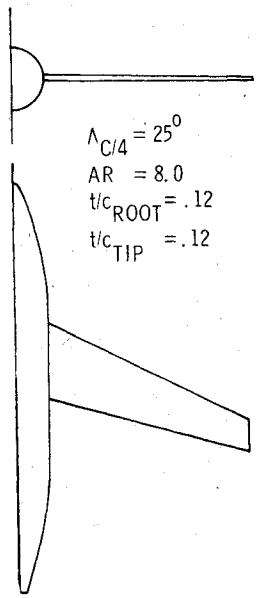

Fig. 7 Lockheed-Georgia/AFOSR wing "A" test case configuration.

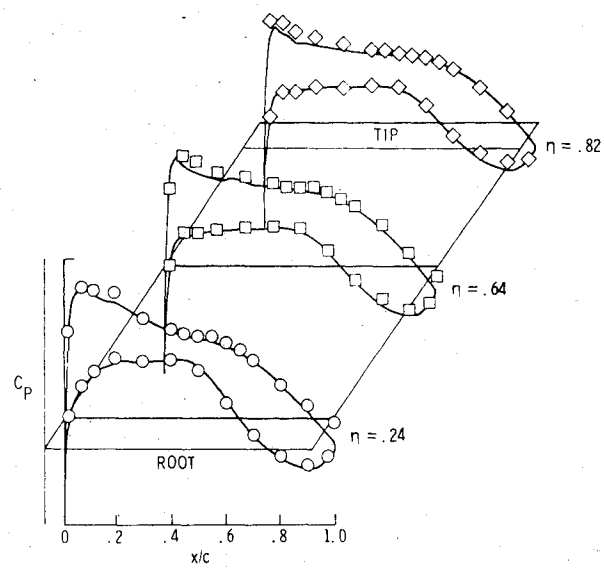

Fig. 8 Chordwise pressure distributions, advanced transport configuration.

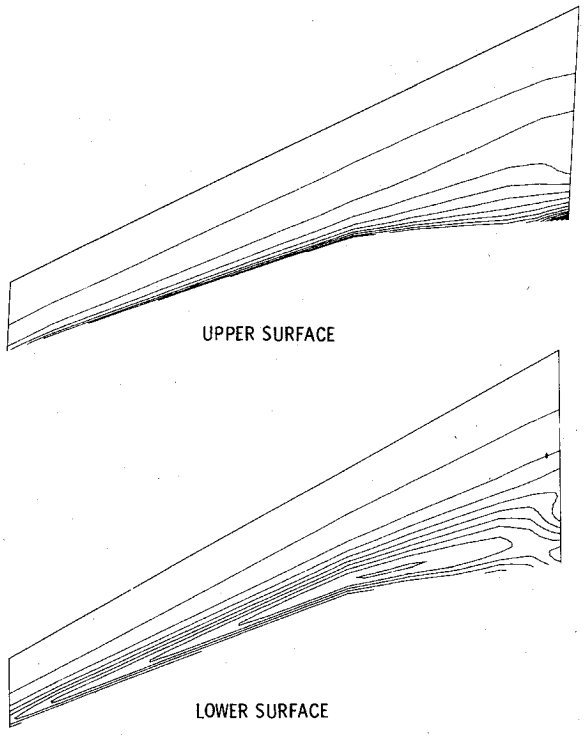

Fig. 9 δ^* isoinclines.

experimental angle of attack of 1.65 deg and Mach number of 0.78; the Reynolds number was 2.4×10^6, based on the mean chord.

Computed chordwise pressure distributions, taken at 24, 64, and 82% semispan, are compared with experiment in Fig. 8. The experimental stations are 26, 63, and 82% semispan. Agreement again is good, with cove region and trailing-edge pressure predictions quite reasonable. Discrepancies at the upper surface leading edges of the outboard stations are noted. No explanation can be given at this time.

Isoinclines of δ^* for the test case just described are shown in Fig. 9 for the upper and lower surfaces, respectively. Note that on the upper surface, lines of constant δ^* run for the most part parallel to the leading edge, indicating little cross flow in the boundary layer. Near midspan, however, δ^* grows very rapidly as the trailing edge is approached, as compared to the inboard region. This strongly reduces the trailing-edge angle of the displacement body, effectively decambering this region more than inboard. Isoinclines of δ^* on the lower surface are seen to sweep forward from parallel to the leading edge after midchord, indicating more rapid relative thickening of the boundary layer toward the tip. In fact, the maximum δ^*/c in the lower surface cove region is more than 30% thicker in the outboard region than inboard. This reflects the cross flow in the boundary layer causing mass to build up toward the tip; the outboard sections are thus decambered more by viscous effects.

In Fig. 10 is shown a comparison of the section lift distribution over the span, from a purely inviscid calculation using FLO-30 and an interacted calculation using the curved wake model outlined in the previous section. FLO-30 was the inviscid method used in the interacted calculation. Also shown on the figure are experimental section C_ℓ's from integrated pressure distributions of those stations. Apparent from the figure is the large decrease in lift due to the decambering effect of the boundary layer. Also note that this decambering is stronger toward the tip than near the root. A large amount of spanwise flow occurred in the boundary layer in the lower surface cove region, so this effect was expected. The interaction method with the full-wake model agrees well with experiment, with a small discrepancy near the body. This

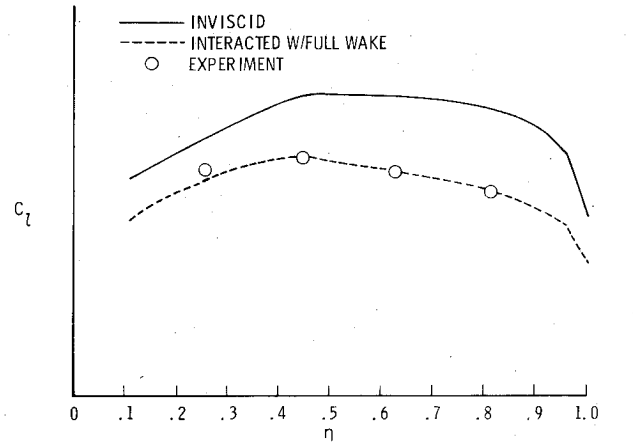

Fig. 10 Spanwise lift distribution, advanced transport configuration.

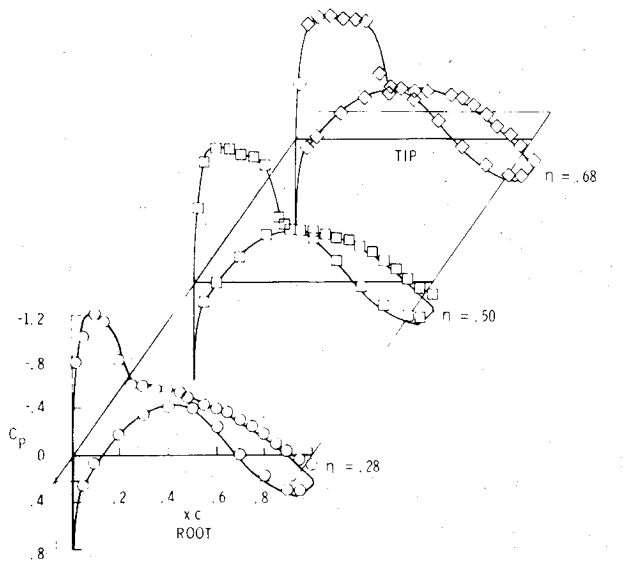

Fig. 11 Chordwise pressure distributions, wing "A" test configuration.

difference is probably due to incorrect modeling of the flow in the wing-body juncture region. The total lift coefficient computed for the wing-body configuration is also within 0.001 of that from experimental balance data.

Flow about the second test case configuration was computed using the interaction procedure with FLO-30, the integral boundary-layer scheme, and the full wake model. Experimental freestream conditions were again used; the Mach number was 0.819, the angle of attack was 1.96 deg, and the Reynolds number was 6×10^6 based on the mean chord. Transition was fixed at 5% chord.

In Fig. 11 is shown a comparison of chordwise pressure distributions, between the data of Ref. 22 and those computed using the interaction procedure. Shock strength and position are predicted well over most of the span, with a disagreement in position of a few percent chord developing toward the tip. Cove region pressures on the lower surface are also predicted reasonably well. Trailing-edge pressures are predicted slightly too high. However, the airfoil sections used in this wing have sharp trailing edges, so this discrepancy cannot be attributed to inadequate modeling of blunt trailing-edge flow. These results are perhaps a good case for the development of an adequate three-dimensional strong interaction theory for wing trailing edges.

As for the advanced transport configuration test case, viscous effects for the wing "A" test case are fairly large, as can be seen in the comparison of interacted and inviscid

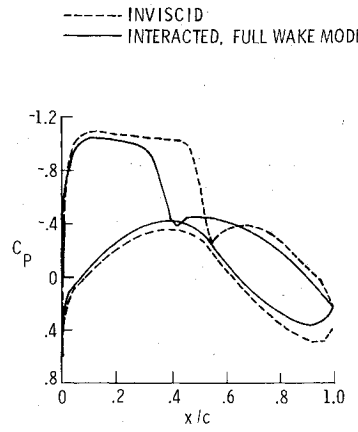

Fig. 12 Comparison of chordwise pressure distribution, inviscid and interacted results, $\eta = 0.68$.

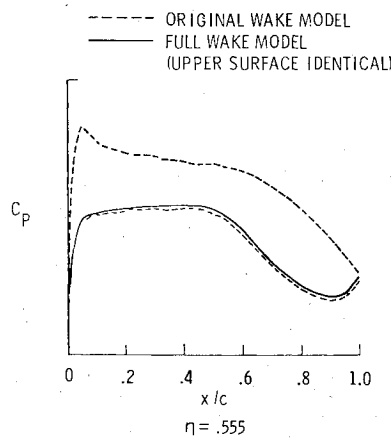

Fig. 14 Chordwise pressure distributions, comparison of wake models, advanced transport configuration, $\eta = 0.56$.

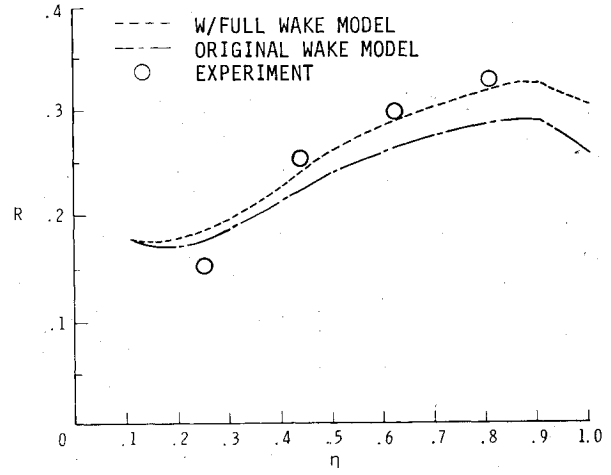

Fig. 13 Lift reduction parameter vs span, advanced transport configuration.

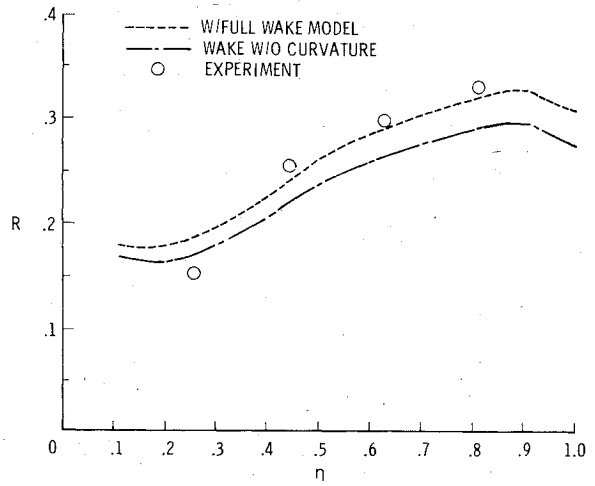

Fig. 15 Effect of wake model on lift reduction parameter vs span.

pressure distribution shown in Fig. 12. Without viscous correction, FLO-30 predicts the shock 14% c too far aft and predicts a much greater cove region pressure.

Wake Effects

The results of calculations including wake effects were compared with those using the wake model of Ref. 15. The wake model in that procedure is modified from that incorporated in the original FLO codes only in the carrying of the trailing-edge thickness downstream to the edge of the computational domain along the assumed wake centerline. Flow tangency is not strictly satisfied at the wake, and the pressures on either side of the wake are set equal only to the order of small-disturbance theory.

In Fig. 13 is plotted the parameter R vs span distance, where

$$R \equiv \frac{C_{\ell_{\text{inviscid}}} - C_\ell}{C_{\ell_{\text{inviscid}}}}$$

R is then the normalized lift reduction due to viscous effects. The two curves shown are computed using the present full wake model and using the model of Ref. 15. Also shown are experimental values of R, computed using the experimental section C_ℓ's and computed inviscid C_ℓ's. Wake effects are thus seen to be very important in the calculation of the lift distribution on three-dimensional wings. The curvature effect of the wake is seen to be larger than the displacement effect, similar to the results shown in two dimensions in Ref. 1.

In Fig. 14 are compared the chordwise pressure distributions near midspan from calculations using the full and original wake models. Note that the cove region pressure predicted using the full wake model is lower than that of the original model, in better agreement with experiment.

In Fig. 15 are compared the spanwise distributions of the lift reduction parameter R, computed using the present wake model, and using the displacement thickness of the wake only; i.e., neglecting the wake curvature effects. The experimental points are again shown. Note that the wake curvature effects are strongest again near the tip and that agreement in this area is much improved by including these effects.

Concluding Remarks

A viscous-inviscid interaction computational method has been developed for three-dimensional transonic wing-body configurations. The procedure employs a three-dimensional integral boundary-layer method which produces results in good agreement with a finite-difference method in a fraction of the computer time. The integral method is stable and robust, and incorporates a model for computation in a small region of streamwise separation. A strip wake model, accounting for thickness and curvature effects, is also included in the interaction procedure. Computation time spent in converging an interacted result is, in many cases, only a small amount greater than to converge an inviscid calculation to the same maximum residual.

Results for test cases in which viscous effects are large show good agreement with experimental data. In particular, the use

of the full-wake model improved the prediction of spanwise load distribution and cove region pressure over results using the wake model originally employed in FLO-30. For wing-body configurations, it is also apparent that body effects may be large. Also, it is seen that a three-dimensional boundary-layer method must be used on the wing, rather than a strip two-dimensional method, in order to predict properly the increased decambering of the sections near the tip due to cross flow in the boundary layer.

Acknowledgments

The author thanks N. Duane Melson of the Theoretical Aerodynamics Branch, NASA Langley Research Center, for invaluable assistance in the final preparation of the manuscript and figures.

References

[1] Melnik, R. E., Chow, R. and Mead, H. R., "Theory of Viscous Transonic Flow Over Airfoils at High Reynolds Numbers," AIAA Paper 77-680, 1977.

[2] Stock, H. W., "Integral Method for the Calculation of Three-Dimensional, Laminar and Turbulent Boundary Layers," NASA TM 75320, 1978.

[3] Smith, P. D., "An Integral Prediction Method for Three-Dimensional Compressible Turbulent Boundary Layers," Royal Aeronautical Establishment R&M 3739, 1974.

[4] Tetervin, N. and Lin, C. C., "A General Integral Form of the Boundary-Layer Equations for Incompressible Flow with an Application to the Calculation of the Separation Point of Turbulent Boundary Layers," NACA TR 1046, 1951.

[5] Mager, A., "Generalization of Boundary Layer Momentum Integral Equations to Three-Dimensional Flows," NACA TR 1067, 1952.

[6] Schlichting, H., *Boundary Layer Theory,* 6th ed., McGraw-Hill Book Co., New York, 1968.

[7] Green, J. E., Weeks, D. J., and Brooman, J. W. F., "Prediction of Turbulent Boundary Layers and Wakes in Compressible Flow by a Lag-Entrainment Method," Aeronautical Research Council R&M 3791, 1977.

[8] Myring, D. F., "An Integral Prediction Method for Three-Dimensional Turbulent Boundary Layers in Incompressible Flow," Royal Aeronautical Establishment TR 70147, 1970.

[9] Roache, P. J., *Computational Fluid Dynamics,* Hermosa Publishers, N. Mex., 1976.

[10] Cumpsty, N. A. and Head, M. R., "The Calculation of Three-Dimensional Turbulent Boundary Layers. Part II: Attachment Line Flow on an Infinite Swept Wing," *Aeronautical Quarterly,* Vol. XVIII, May 1967, p. 150.

[11] McLean, J. D. and Randall, J. L., "Computer Program to Calculate Three-Dimensional Boundary Layer Flows Over Wings With Wall Mass Transfer," NASA CR 3123, 1979.

[12] Stanewsky, E., Puffert, W., Muller, R., and Bateman, T. E. B., "Supercritical Airfoil CAST 7—Surface-Pressure, Wake and Boundary Layer Measurements," AGARD-AR-138, 1979.

[13] Caughey, D. A., Newman, P. A., and Jameson, A., "Recent Experiences with Three-Dimensional Transonic Potential Flow Calculations," NASA TM 78733, 1978.

[14] Jameson, A. and Caughey, D. A., "A Finite Volume Method for Transonic Potential Flow Calculations," AIAA Paper 77-635, July 1977.

[15] Caughey, C. A. and Jameson, A., "Recent Progress in Finite Volume Calculations for Wing-Fuselage Combinations," AIAA Paper 79-1513, July 1979.

[16] Jameson, A., "Iterative Solution of Transonic Flows Over Airfoils and Wings, Including Flows at Mach 1," *Communications on Pure and Applied Mathematics,* Vol. 27, May 1974, pp. 283-309.

[17] Lock, R. C., "Calculation of Viscous Effects on Aerofoils in Compressible Flow," Royal Aeronautical Establishment Tech. Memo. Aero. 1646, Sept. 1975.

[18] Moore, F. K., "Displacement Effect of a Three-Dimensional Boundary Layer," NACA TR 1124, March 1952.

[19] Kjelgaard, S. O. and Thomas, J. L., "Comparison of Three-Dimensional Panel Methods with Strip Boundary Layer Simulations to Experiment," NASA TM 80088, July 1979.

[20] Bartlett, D. W., "Wind Tunnel Investigations of Several High Aspect-Ratio Supercritical Wing Configurations on a Wide-Body Fuselage," NASA TM X-71996, 1977.

[21] Waggoner, E. G., "Computational Transonic Analysis for a Supercritical Transport Wing-Body Configuration," AIAA Paper 80-0129, Jan. 1980.

[22] Hinson, B. L. and Burdges, K. P., "Acquisition and Application of Transonic Wing and Far-Field Test Data for Three-Dimensional Computational Method Evaluation," Air Force Office of Scientific Research, AFOSR TR-80-0421, 0422, March 1980.